

Evaluation of particle statistics in powder diffractometry by a spinner-scan method

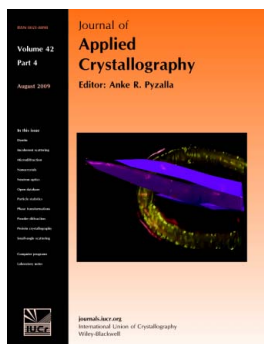
T. Ida, T. Goto and H. Hibino

J. Appl. Cryst. (2009). **42**, 597–606

Copyright © International Union of Crystallography

Author(s) of this paper may load this reprint on their own web site or institutional repository provided that this cover page is retained. Reproduction of this article or its storage in electronic databases other than as specified above is not permitted without prior permission in writing from the IUCr.

For further information see <http://journals.iucr.org/services/authorrights.html>



Many research topics in condensed matter research, materials science and the life sciences make use of crystallographic methods to study crystalline and non-crystalline matter with neutrons, X-rays and electrons. Articles published in the *Journal of Applied Crystallography* focus on these methods and their use in identifying structural and diffusion-controlled phase transformations, structure–property relationships, structural changes of defects, interfaces and surfaces, *etc.* Developments of instrumentation and crystallographic apparatus, theory and interpretation, numerical analysis and other related subjects are also covered. The journal is the primary place where crystallographic computer program information is published.

Crystallography Journals **Online** is available from journals.iucr.org

Evaluation of particle statistics in powder diffractometry by a spinner-scan method

T. Ida,* T. Goto and H. Hibino

Ceramics Research Laboratory, Nagoya Institute of Technology, Asahigaoka, Tajimi 507-0071, Japan. Correspondence e-mail: ida.takashi@nitech.ac.jp

Received 2 March 2009
Accepted 28 May 2009

The uncertainty in measured diffraction intensities caused by particle statistics, which originates from the limited number of crystallites satisfying the diffraction condition, has been evaluated by a step-scan measurement about the rotation angle of a specimen-spinning attachment of a laboratory powder X-ray diffractometer. The residual statistical variance of the spinner-scan intensity data, after subtraction of periodic drift and variance caused by counting statistics, was assigned to the variance caused by particle statistics. Particle statistics for a standard Si powder (NIST SRM640c) and three size fractions (nominally 3–7, 8–12 and 18–22 μm in Stokes diameter) of quartz powder separated by a sedimentation method have been analysed by scanning electron microscopy (SEM) and the spinner-scan method using a powder X-ray diffractometer. It has been confirmed that the observed ratio of the squared diffraction-peak intensity to the variance caused by particle statistics is proportional to the multiplicity of reflections predicted by the crystal structure. The spinner-scan intensity data for the standard Si powder (NIST SRM640c), the effective particle diameter of which was estimated at 5.6 μm by SEM image analysis, was used as the standard for crystallite-size evaluation of quartz powder based on analysis of spinner-scan data. The effective crystallite diameters of the three quartz powder samples have been estimated at 6.5 (2), 11.7 (2) and 22.8 (2) μm by the analysis of the spinner-scan data, while the effective particle diameters evaluated by SEM image analysis are 7.1, 12 and 25 μm , respectively. Other possible applications of the analysis of particle statistics based on the spinner-scan method are also discussed.

© 2009 International Union of Crystallography
Printed in Singapore – all rights reserved

1. Introduction

It is known that the statistical uncertainty in measured X-ray diffraction intensity data originates mainly from counting statistics and particle statistics. The errors caused by counting statistics can be simply approximated by the square root of the measured number of counts, when the count rate is sufficiently lower than the reciprocal of the response time of the detection system. One of the authors recently proposed a practical method to evaluate the statistical errors affected by the finite response time of X-ray detection systems (Ida, 2008).

In contrast to counting statistics, which are a general issue in various fields using nuclear counting, photon counting and neural counting (Teich, 1985), particle statistics are a problem peculiar to powder diffractometry.

In the pioneering work on this subject by Alexander *et al.* (1948), a theoretical framework for particle statistics has almost been established. The relative deviation of the diffraction intensity caused by the restricted number of diffracting crystallites is simply given by

$$\Delta I_{\text{particle}}/\langle I \rangle = 1/n_{\text{eff}}^{1/2}, \quad (1)$$

where n_{eff} is the effective number of crystallites that satisfy the diffraction condition. The effective number n_{eff} is connected to the total number of irradiated crystallites N and the probability p that each crystallite satisfies the diffraction condition, that is, $n_{\text{eff}} = Np$ when p is much less than unity.

The total irradiated number of crystallites N is given by

$$N = fV/v_{\text{eff}}, \quad (2)$$

where f is the filling factor of the powder sample and V is the irradiated volume, which is given by

$$V = A\mu^{-1} \quad (3)$$

for the cross section of the X-ray beam A and the linear absorption coefficient of the specimen μ , when the diffraction intensity data are measured using a divergence slit with a fixed open angle in symmetric reflection mode.

The effective particle volume v_{eff} in equation (2) is defined by the ratio of the mean squared volume to the mean volume of the crystallites,

$$v_{\text{eff}} = \langle v^2 \rangle / \langle v \rangle, \quad (4)$$

when the crystallite size distribution is taken into account (Alexander *et al.*, 1948).

Since the linear absorption coefficient μ of a powder with filling factor f is given by $\mu = f\mu_0$ for the bulk linear absorption coefficient μ_0 , the total irradiated number N is independent of the filling factor, and equation (2) can be reduced to

$$N = A/\mu_0 v_{\text{eff}}. \quad (5)$$

The probability p for randomly oriented crystallites in stationary specimens can be approximated by

$$p = m_{\text{eff}} \Delta\omega \Delta\chi / 4\pi, \quad (6)$$

where m_{eff} is the effective multiplicity of reflection, and $\Delta\omega$ and $\Delta\chi$ are the tolerance angles for the normal orientation of the diffraction plane to deviate along the equatorial and axial directions, respectively (de Wolff, 1958).

When the effect of a rotating specimen is simplified as the expansion of the tolerance area from that of a rectangle, $\Delta\omega \Delta\chi$, to a circle, $\pi(\Delta\chi)^2/4$, the probability p for crystallites in a rotating specimen will be given by

$$p = m_{\text{eff}} (\Delta\chi)^2 / 16. \quad (7)$$

The effective multiplicity m_{eff} is defined for an overlapped reflection with component multiplicity m_j and intensity I_j by the following equation (Alexander *et al.*, 1948):

$$m_{\text{eff}} = \left(\sum_j m_j I_j \right)^2 / \sum_j m_j I_j^2. \quad (8)$$

The tolerance angles $\Delta\omega$ and $\Delta\chi$ are given by

$$\Delta\omega = w/R, \quad (9)$$

$$\Delta\chi = h/2R \sin \theta, \quad (10)$$

where R is the goniometer radius, θ is the Bragg angle, and w and h are the effective width and length, respectively, of the line focus of the X-ray source (de Wolff, 1958).

Although the above formulae were originally intended to describe the statistical properties of the integrated intensity of a diffraction peak (Alexander *et al.*, 1948), they can also be applied to peak intensity, by modifying only the interpretation of the effective width w (de Wolff, 1958). The effective width w of the peak intensity is predominantly determined by the geometry of the X-ray source, but it may also be affected by the spectroscopic width of the X-ray beam and the width of the receiving slit under the restrictions of the diffraction condition. The effective length h is considered to be determined by the open angle Φ_A of the Soller slits, which are commonly adopted in modern Bragg–Brentano diffractometers, as $h = R\Phi_A$ (Smith, 2001).

In a typical case of $R = 185$ mm, $w = 0.1$ mm and $\Phi_A = 5.0^\circ$, the probabilities of crystallites in stationary and rotating specimens satisfying the diffraction condition at a fixed rocking angle are estimated at $p = 6.0 \times 10^{-5}$ and 1.5×10^{-2} , respectively, for the 111 reflection of Si with multiplicity $m = 8$ at the diffraction angle $2\theta = 28.4^\circ$, and the relative errors caused by particle statistics for $5 \mu\text{m}$ crystallites in an irra-

diated volume of $V = 3 \text{ mm}^3$ will be about $\Delta I_{\text{particle}}/I = 1.9$ and 0.12%, respectively.

It should be emphasized that the improved accuracy obtained by rotating the specimen is mainly caused by the geometry of the diffractometer, where the tolerance angle for the normal orientation of the diffraction plane along the axial direction, $\Delta\chi = \Phi_A/2\sin\theta$, is much more generous than that along the equatorial direction, $\Delta\omega = w/R$.

Since the aspect ratio $\Delta\chi/\Delta\omega$ is greater than 100 for lower-angle diffraction peaks, it is expected that a slight rotation of the specimen by about 1° has a similar effect to refilling the crystalline powder in the sample holder. It is suggested that quantitative analysis of particle statistics can be achieved by simply recording the variation in the diffraction intensities on rotation of the specimen.

In this study, we have conducted step-scan diffraction intensity measurements of Si and quartz crystalline powder samples with rotation of the specimen at fixed diffraction angles, and examined the validity of the application of the theory proposed by Alexander *et al.* (1948) to intensity data collected at a fixed rocking angle. It will be shown that quantitative evaluation of crystallite sizes larger than $1 \mu\text{m}$ is enabled by applying this method. Other possible applications of the method are also discussed.

2. Experimental

2.1. Samples

Standard Si powder (NIST SRM640c) was used without further grinding or sieving. The median particle size of the Si powder, determined by a laser scattering method, was reported to be $4.9 \mu\text{m}$ in the certificate (Freiman & Trahey, 2000).

Three fractions of quartz powder samples were prepared by separating crushed and ground Brazilian quartz crystals by a sedimentation method. The nominal Stokes diameters of the three quartz samples were 3–7, 8–12 and 18–22 μm .

2.2. SEM image analysis

Scanning electron microscopy (SEM) images of powder samples were taken with a field-emission-type scanning electron microscope (Jeol JSM-7000F). Particle images were extracted from SEM images with the aid of computer software for image analysis (*Scion Image*; Scion Corporation, Maryland, USA). The numbers of extracted particle images were 1049 for Si, and 1134, 1049 and 1391 for the 3–7, 8–12 and 18–22 μm fractions of quartz powder, respectively.

The size of each crystallite was specified as the diameter of a circle with the same area as the particle image.

2.3. Spinner-scan measurements

A sample holder with a cylindrical hollow of $\varphi = 30$ mm in diameter and 0.6 mm in depth was filled with the powder samples. A home-made specimen spinner attached to a conventional powder diffractometer (Rigaku RAD-2C) with a goniometer radius of $R = 185$ mm was used for step-scan

Table 1

Reflections measured by the spinner-scan method.

hkl is the index of reflection, m_{eff} is the effective multiplicity of reflection, FT_0 is the measurement time per step for Si, and FT_1 , FT_2 and FT_3 are those for the 3–7, 8–12 and 18–22 μm quartz samples, respectively.

Si (NIST SRM640c)			α -quartz				
hkl	m_{eff}	FT_0 (s)	hkl	m_{eff}	FT_1 (s)	FT_2 (s)	FT_3 (s)
111	8	0.5	100	6	1	1	1
220	12	1	101/011	9.85	0.5	0.5	0.5
311	24	2.5	110	6	2	2	2
400	6	3	102/012	8.23	3	2	2
331	24	6.5	111/11 $\bar{1}$	12	5	4	5
422	24	5.5	200	6	3	3	3
333/511	32	12.5	201/021	10.39	5	5	5
440	12	8.5	112/11 $\bar{2}$	12	1.5	1.5	1.5
531	48	18	202/022	9.24	5	5	5
620	24	10	103/013	6.01	12	9	10
533	24	19	211/121	23.72	3	3	3

measurements about the rotation angle of the specimen. A Cu target sealed tube operating at 40 kV and 30 mA was used as the X-ray source. The take-off angle of the source X-ray beam from the Cu target was about 4° and the effective width of the X-ray source was estimated at $w = 0.12$ mm from the 2Θ -scan intensity profile of the direct beam. The divergence/scattering slit open angles were fixed at $\Phi_{\text{DS/SS}} = 1^\circ$ and a receiving slit of width 0.15 mm was used. The width of the X-ray beam, measured by locating a fluorescent plate at the specimen position, was $W_{\text{beam}} = 10$ mm. The cross section of the beam at the specimen position was estimated at $A = W_{\text{beam}}R\Phi_{\text{DS/SS}} = 32$ mm². A curved graphite monochromator attached on the diffracted-beam side of the goniometer was adjusted for Cu $K\alpha$ wavelength.

400 diffraction intensity data were recorded by rotating the specimen stepwise with an interval of 0.9° over 360° , for each of 11 diffraction peaks at $2\Theta/\Theta$ angles fixed at the peak top positions. The measurement time per step was varied for different reflections, so that at least several hundred counts were collected for each measurement step. The hkl indices of the measured reflections, the effective multiplicity m_{eff} and the measurement time are listed in Table 1. The effective multiplicity of reflection was estimated based on the results of Rietveld analysis using the program *RIETAN* developed by Izumi & Ikeda (2000).

3. Results and discussion

3.1. SEM images

Typical SEM images of the Si (NIST SRM640c) and three fractions of α -quartz powder samples are shown in Figs. 1 and 2. Extracted particle images of the Si sample are illustrated in the lower panel of Fig. 1.

The cumulative volume distribution of Si powder obtained by SEM image analysis is plotted in Fig. 3. Since the observed size distribution could not be reasonably fitted by any of the log-normal, Γ or Weibull distributions, it was fitted by a modified formula of a Γ -distribution function given by

$$F_{\Gamma W}(D) = -\rho + (1 + \rho)P[\alpha + 3/\beta; (D/D_0)^\beta], \quad (11)$$

where ρ is the missing volume fraction of particles smaller than the measurable size, D_0 is a scale parameter, and α and β are shape parameters for the model function (see Appendix A). The normalized incomplete Γ function $P(\alpha; x)$ is defined by

$$P(\alpha; x) \equiv \frac{1}{\Gamma(\alpha)} \int_0^x t^{\alpha-1} \exp(-t) dt, \quad (12)$$

$$\Gamma(\alpha) \equiv \int_0^\infty t^{\alpha-1} \exp(-t) dt.$$

It should be noted that the formula of equation (11) reduces to the usual Γ distribution for $\beta = 1$ and to the Weibull distribution for $\alpha = 1$.

The optimized values of the fitting parameters are $\rho = 0.0077$ (4), $D_0 = 5.63$ (7) μm , $\alpha = 0.210$ (17) and $\beta = 3.57$ (9), where the error values in parentheses are estimated by

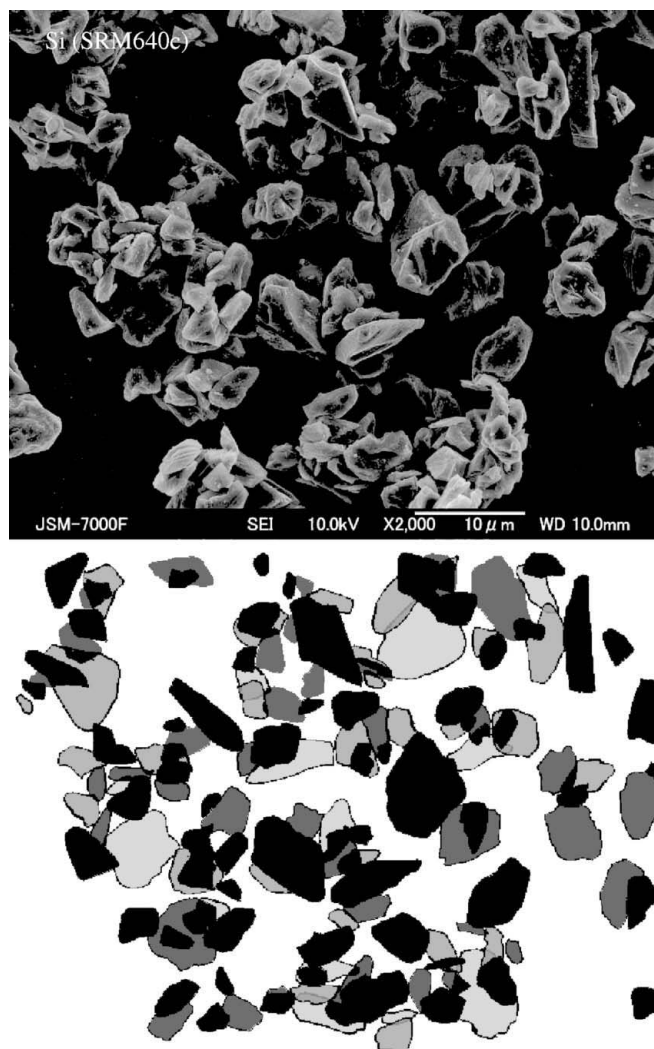


Figure 1
SEM image of standard Si powder (NIST SRM640c) (upper panel) and the extracted particle profiles (lower panel).

assuming a fixed value of error $\Delta D = 0.1 \mu\text{m}$ in the measured diameter. As a result, it can be assumed that the missing

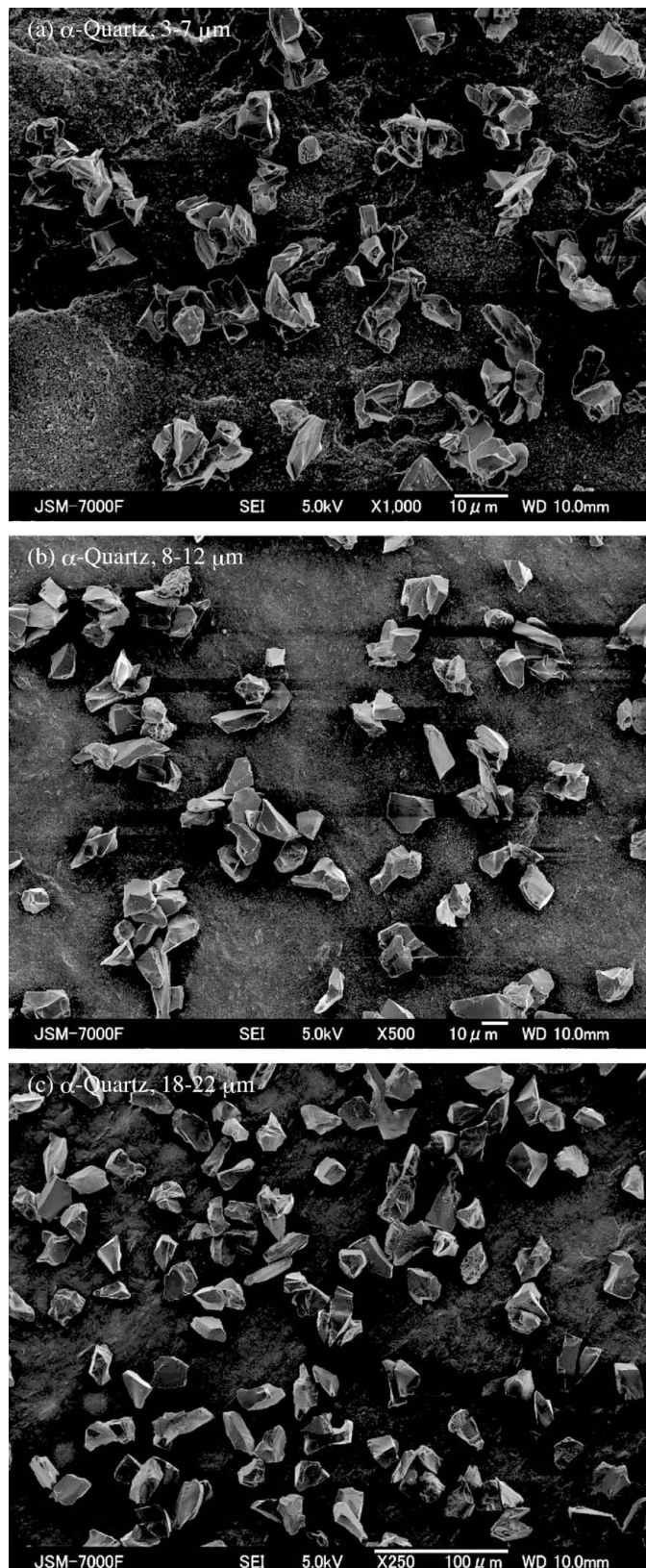


Figure 2
SEM images of (a) 3–7 μm , (b) 8–12 μm and (c) 18–22 μm fractions of α -quartz powder.

fraction ρ is negligible, similar to the assumption applied in the work of Alexander *et al.* (1948). The effective diameter of the Si powder, defined by $D_{\text{eff}} \equiv (6v_{\text{eff}}/\pi)^{1/3}$, is estimated directly from the raw data $\{D_j\}$ by the equation

$$(D_{\text{eff}})_{\text{raw}} = \left(\frac{\sum_j D_j^6}{\sum_j D_j^3} \right)^{1/3}, \quad (13)$$

and from the fitting parameters D_0 , α and β by the equation

$$(D_{\text{eff}})_{\text{fit}} = D_0 \left[\frac{\Gamma(\alpha + 6/\beta)}{\Gamma(\alpha + 3/\beta)} \right]^{1/3}. \quad (14)$$

The effective diameter of the Si powder was estimated at $(D_{\text{eff}})_{\text{raw}} = 5.6 \mu\text{m}$ from the raw data and also at $(D_{\text{eff}})_{\text{fit}} = 5.6 \mu\text{m}$ from the fitting parameters.

The median diameter for the volume distribution of SRM640c numerically evaluated from the raw data of measured diameter, and from the curve calculated using the optimized fitting parameters, were 5.3 and 5.2 μm , respectively, while the value reported in the certificate of SRM640c is 4.9 μm .

The diameter evaluated by the current method may be slightly overestimated, because the unknown diameter along the viewing direction on capturing a SEM image is assumed to be equal to the diameter of a circle with the same area as the particle image, while it is expected that non-spherical particles tend to adhere, making the shortest diameter normal to the face of the substrate. However, the effective diameter of Si is assumed to be $(D_{\text{eff}})_{\text{Si}} = 5.6 \mu\text{m}$ in this study.

The cumulative volume distributions of quartz powder obtained by SEM image analysis are plotted in Fig. 4. The volume distributions of the quartz samples are satisfactorily fitted by a model based on the log-normal distribution, which is given by

$$F_{\text{LN}}(D) = -\rho + \frac{1 + \rho}{2} \left\{ 1 + \operatorname{erf} \left[\frac{\ln D - \ln D_m - 3\omega^2}{(2\omega)^{1/2}} \right] \right\}, \quad (15)$$

where ρ is the missing volume fraction of particles smaller than the measurable size, D_m is the median diameter and ω is

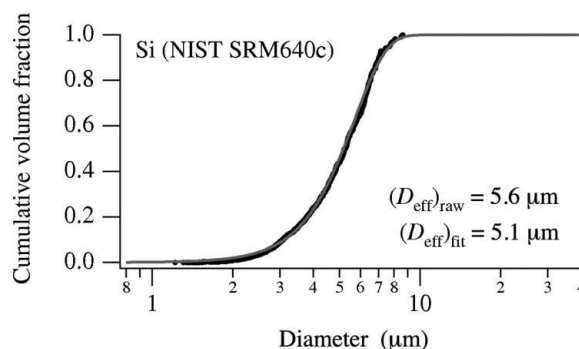


Figure 3
Cumulative particle-size distribution of Si (NIST SRM640c), plotted as black dots, and the optimized modified Γ -distribution curve (grey line) calculated with the parameters $D_0 = 5.63 \mu\text{m}$, $\alpha = 0.210$ and $\beta = 3.57$.

the logarithmic standard deviation. The error function $\text{erf}(x)$ is defined by

$$\text{erf}(x) \equiv \frac{2}{\pi^{1/2}} \int_0^x \exp(-t^2) dt. \quad (16)$$

Table 2 lists the values of the optimized fitting parameters and effective diameters, $(D_{\text{eff}})_{\text{raw}}$ and $(D_{\text{eff}})_{\text{fit}}$. The effective diameter $(D_{\text{eff}})_{\text{fit}}$ is calculated from the optimized fitting parameters D_m and ω for the log-normal distribution by the equation

$$(D_{\text{eff}})_{\text{fit}} = D_m \exp(9\omega^2/2) \quad (17)$$

(see Appendix B).

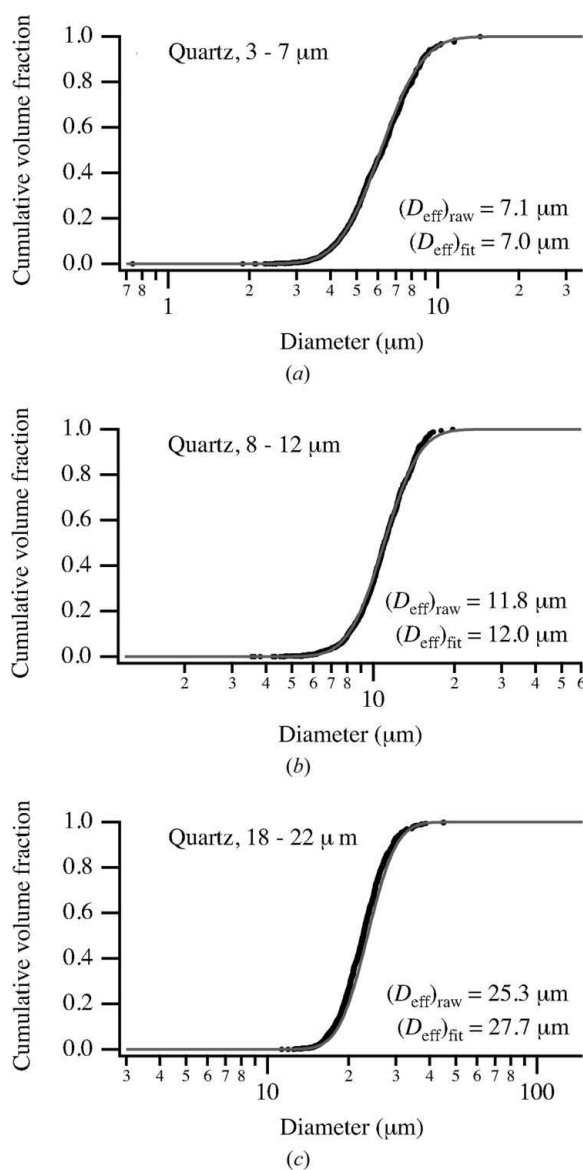


Figure 4
Cumulative particle-size distribution of (a) 3–7 μm , (b) 8–12 μm and (c) 18–22 μm fractions of α -quartz powder. Measured diameters are plotted as black dots, and the optimized log-normal distribution curves, calculated with optimized parameters, are drawn as grey lines.

Table 2

Results of SEM image analysis of quartz powder.

ΔD is the assumed error in the measured diameter, ρ is the missing volume fraction below the measurable size, D_m is the median diameter, ω is the logarithmic standard deviation, and $(D_{\text{eff}})_{\text{raw}}$ and $(D_{\text{eff}})_{\text{fit}}$ are the values of the effective diameter evaluated from raw data and optimized fitting parameters, respectively.

Stokes diameter (μm)	3–7	8–12	18–22
ΔD (μm)	0.2	0.4	0.8
ρ	–0.0009 (0)	–0.0000 (0)	–0.0003 (0)
D_m (μm)	4.831 (6)	9.239 (18)	21.03 (2)
ω	0.2836 (11)	0.2400 (12)	0.1937 (11)
$(D_{\text{eff}})_{\text{raw}}$ (μm)	7.1	11.8	25.3
$(D_{\text{eff}})_{\text{fit}}$ (μm)	7.0	12.0	27.7

3.2. Spinner-scan data of Si powder

The observed spinner-scan intensity profile of the Si 111 reflection is shown in Fig. 5. Periodic drift in the observed intensity profile, which is likely to be caused by slight misalignment of the sample face, is modelled by Fourier expansion up to the second order. The Fourier coefficients $\{c_k\}$ are calculated by

$$c_k = n^{-1} \sum_{j=0}^{n-1} I_j \exp(-2\pi i k j / n) \quad (18)$$

from the observed intensity data $\{I_j\}$ ($j = 0, \dots, n-1$), and the profile of the periodic drift $\{(I_{\text{drift}})_j\}$ is approximated by

$$(I_{\text{drift}})_j = \sum_{k=-2}^2 c_k \exp(2\pi i k j / n). \quad (19)$$

The calculated drift profile is also shown in Fig. 5.

The average intensity $\langle I \rangle$ is straightforwardly given by the zeroth-order Fourier coefficient c_0 . The statistical variance of the residuals $(\delta I)_j = I_j - (I_{\text{drift}})_j$ is calculated by

$$(\Delta I_{\text{obs}})^2 = (n-5)^{-1} \sum_{j=0}^{n-1} (\delta I)_j^2, \quad (20)$$

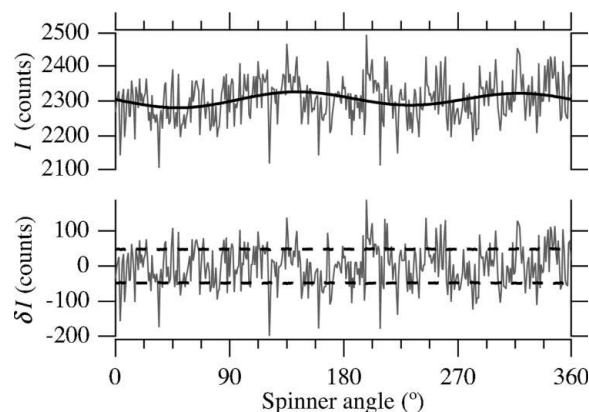


Figure 5

Spinner-scan intensity profile of the Si 111 reflection. The raw intensity data I and assumed drift I_{drift} are drawn as grey and black lines, respectively, in the upper panel. The lower panel shows the deviation $\delta I = I - I_{\text{drift}}$ (grey line) and the \pm standard deviation predicted by counting statistics (broken lines).

Table 3

Results of spinner-scan measurements for Si powder (NIST SRM640c).

$\langle I \rangle$ is the average intensity, $(\Delta I_{\text{obs}})^2$ is the observed statistical variance, $(\Delta I_{\text{particle}})^2$ is the statistical variance assigned to particle statistics, n_{eff} is the effective number of diffracting crystallites, D'_{eff} is the effective diameter calculated from assumed values of geometric parameters of the diffractometer and D_{eff} is the calibrated value of the effective diameter.

<i>hkl</i>	2θ (°)	$\langle I \rangle$	$(\Delta I_{\text{obs}})^2$	$(\Delta I_{\text{particle}})^2$	n_{eff}	D'_{eff} (μm)	D_{eff} (μm)
111	28.59	2304 (3)	3440 (260)	1140 (260)	4670 (1100)	4.1 (3)	5.0 (4)
220	47.44	2579 (3)	4890 (340)	2310 (340)	2900 (440)	4.6 (2)	5.2 (3)
311	56.26	3266 (4)	7140 (470)	3880 (470)	2750 (340)	5.6 (2)	6.1 (3)
400	69.24	1211 (3)	2720 (180)	1510 (180)	970 (120)	4.7 (2)	5.0 (2)
331	76.48	4157 (5)	9680 (690)	5520 (690)	3130 (400)	4.9 (2)	5.2 (2)
422	88.12	4532 (5)	10770 (760)	6240 (760)	3290 (410)	4.7 (2)	5.0 (2)
333/511	95.05	5028 (6)	12310 (840)	7290 (840)	3470 (410)	4.9 (2)	5.4 (2)
440	106.79	2344 (4)	5930 (400)	3590 (400)	1530 (180)	4.5 (2)	5.2 (2)
531	114.16	9705 (8)	25800 (2000)	16100 (2000)	5860 (740)	4.6 (2)	5.4 (2)
620	127.60	5385 (6)	13510 (960)	8100 (960)	3570 (430)	4.2 (2)	5.4 (2)
533	136.92	6821 (6)	16200 (1100)	9400 (1100)	4950 (600)	3.7 (2)	5.2 (2)

where the degree of freedom is assumed to be decreased by five, because the second-order Fourier expansion of real data includes five independent coefficients determined by the source data. The errors in the evaluated variance, $\Delta[(\Delta I_{\text{obs}})^2]$, were calculated by

$$\{\Delta[(\Delta I_{\text{obs}})^2]\}^2 = \sum_{j=0}^{n-1} \frac{(\delta I_j)^4}{n^2} - \frac{(\Delta I_{\text{obs}})^4}{n} \quad (21)$$

The variance caused by the particle statistics, $(\Delta I_{\text{particle}})^2$, is calculated from the observed variance $(\Delta I_{\text{obs}})^2$ by the equation

$$(\Delta I_{\text{particle}})^2 = (\Delta I_{\text{obs}})^2 - (\Delta I_{\text{count}})^2, \quad (22)$$

where $(\Delta I_{\text{count}})^2$ is the variance caused by the counting statistics, which is approximated by $(\Delta I_{\text{count}})^2 \simeq \langle I \rangle$.

Then, the effective number of diffracting crystallites n_{eff} is calculated by

$$n_{\text{eff}} = \langle I \rangle^2 / (\Delta I_{\text{particle}})^2 \quad (23)$$

for each reflection.

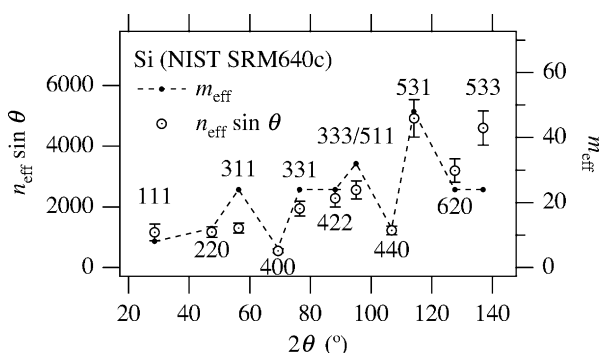


Figure 6

Product of the effective number of crystallites n_{eff} with $\sin \theta$ (open circles) and the known effective multiplicity of reflection m_{eff} for Si (dots connected by broken lines).

The values of the observed average intensity $\langle I \rangle$, the statistical variance $(\Delta I_{\text{obs}})^2$, the statistical variance assigned to the particle statistics $(\Delta I_{\text{particle}})^2$ and the effective number of diffracting crystallites $n_{\text{eff}} = \langle I \rangle^2 / (\Delta I_{\text{particle}})^2$, evaluated for the spinner-scan diffraction intensity data of Si powder (NIST SRM640c), are listed in Table 3.

Fig. 6 shows the values of $n_{\text{eff}} \sin \theta$ calculated from the spinner-scan data, and also the known multiplicity m_{eff} for all measured reflections from Si powder. It is clearly shown that the variation of the experimental values of $n_{\text{eff}} \sin \theta$ is very similar to that of m_{eff} . The observed similarity confirms that the particle statistics have certainly been evaluated by the spinner-scan measurement, because no origin of statistical variation except the particle statistics is likely to cause such behaviour as is proportional to the multiplicity of reflections.

The effective crystallite diameter D'_{eff} is first calculated by

$$D'_{\text{eff}} = \left(\frac{3m_{\text{eff}}Aw\Phi_{\Lambda}}{4\pi^2 n_{\text{eff}} \mu_0 R \sin \theta} \right)^{1/3}, \quad (24)$$

according to the formula for stationary specimens given in equation (6). The values of D'_{eff} for each reflection peak of Si, calculated by assuming $\mu_0 = 142.6 \text{ cm}^{-1}$ and with instrumental parameters $A = 32 \text{ mm}^2$, $w = 0.12 \text{ mm}$, $\Phi_{\Lambda} = 5^\circ$ and $R = 185 \text{ mm}$, are also listed in Table 3.

Fig. 7(a) plots the values of D'_{eff} evaluated for all the measured reflection peaks of Si versus the diffraction angle 2θ .

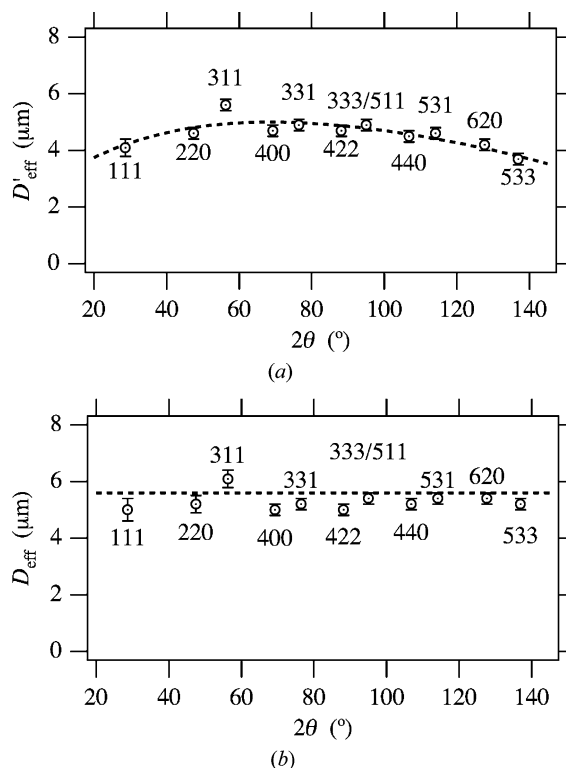


Figure 7

(a) Effective diameter D'_{eff} of Si powder calculated with assumed instrumental parameters (circles) and the fitted curve of $D'_{\text{fit}} = (5.6 \mu\text{m})(0.62/\tan \theta - 0.41 + 1.33 \tan \theta)^{-1/3}$ (broken line). (b) Calibrated effective diameter D_{eff} of Si powder (circles) and the average value of $5.6 \mu\text{m}$ (broken line).

It should be noted that the relative error for the particle diameter is suppressed by a factor of 1/3 from that of the particle volume evaluated directly by the spinner-scan measurement. The weighted average of D'_{eff} is nominally estimated at $\overline{D'}_{\text{eff}} = 4.52$ (6) μm , while the corresponding value estimated by the SEM image analysis is $(D_{\text{eff}})_{\text{Si}} = 5.6$ μm .

At the moment, it is difficult to derive an *a priori* formula for the systematic behaviour of the evaluated effective diameter D'_{eff} depending on the diffraction angle. However, such dependence is likely to be caused by a combination of the neglected spectroscopic distribution of the source X-ray, the finite receiving-slit width and instrumental aberrations, as has been suggested by de Wolff (1958). When the systematic deviation is assumed to be caused predominantly by instrumental effects, it is expected that a common calibration curve can be applied to the intensity data from different samples when they are measured under the same conditions.

Taking into account the uncertainties of the instrumental parameters of the diffractometer on the evaluation of D'_{eff} , and the above systematic deviation, the formula for evaluating the effective diameter D_{eff} should be modified using the equation

$$D_{\text{eff}} = D'_{\text{eff}}(D_{\text{eff}})_{\text{Si}}/(D'_{\text{eff}})_{\text{fit}}, \quad (25)$$

where $(D_{\text{eff}})_{\text{Si}} = 5.6$ μm is the value determined by the SEM image analysis, and $(D'_{\text{eff}})_{\text{fit}}$ is the correction that should be applied to the observed values of D'_{eff} .

In this study, the systematic behaviour of D'_{eff} for the Si data is modelled by the following formula depending on the diffraction angle 2θ ,

$$(D'_{\text{eff}})_{\text{fit}} = (D_{\text{eff}})_{\text{Si}}(t_0/\tan\theta + t_1 + t_2 \tan\theta)^{-1/3}, \quad (26)$$

because it is expected that the effect of spectroscopic broadening is proportional to $\tan\theta$, and the dependence proportional to $1/\tan\theta$ is dominant in the effect of instrumental aberrations (Ida & Toraya, 2002). The optimized values of the fitting parameters are estimated at $t_0 = 0.62$ (19), $t_1 = -0.41$ (45) and $t_2 = 1.33$ (23) by a nonlinear least-squares fitting method. The fitting curve drawn in Fig. 7(a) satisfactorily reproduces the observed systematic behaviour.

The formula to evaluate the calibrated value of the effective diameter D_{eff} is then given by

$$D_{\text{eff}} = \left[\frac{m_{\text{eff}}(138 \mu\text{m}^2)(0.62/\tan\theta - 0.41 + 1.33 \tan\theta)}{\mu_0 n_{\text{eff}} \sin\theta} \right]^{1/3}. \quad (27)$$

The values of the effective diameter D_{eff} calculated by equation (27) are listed in the last column of Table 3 and are also shown in Fig. 7(b). Coincidence of the calibrated values D_{eff} evaluated from different reflections of Si is significantly improved from that of the crude estimation D'_{eff} .

3.3. Spinner-scan data of quartz powder

The spinner-scan intensity data of the three fractions of quartz powder have been analysed in the same manner as the Si powder sample, except that the bulk linear absorption coefficient of $\mu_0 = 89.81$ cm^{-1} is used for the calculation of the

effective number of diffracting crystallites n_{eff} , the known effective multiplicity m_{eff} of α -quartz (see Table 1) is used for the calculation of D'_{eff} , and the calibration curve $(D_{\text{eff}})_{\text{Si}}/(D'_{\text{eff}})_{\text{fit}}$ determined from the Si data is used for the estimation of D_{eff} .

The values of the observed average intensity $\langle I \rangle$, the statistical variance $(\Delta I_{\text{obs}})^2$, the statistical variance assigned to particle statistics $(\Delta I_{\text{particle}})^2$, the effective number of diffracting crystallites $n_{\text{eff}} = \langle I \rangle^2/(\Delta I_{\text{particle}})^2$, and the crude and calibrated effective diameters D'_{eff} and D_{eff} , evaluated for the three fractions of quartz powder, are listed in Tables 4–6.

The calibrated values of the effective diameter D_{eff} for 11 reflections of the three quartz powder samples are plotted in Fig. 8. No significant systematic deviation of D_{eff} is detected, except that the value estimated for the 100 reflection seems to

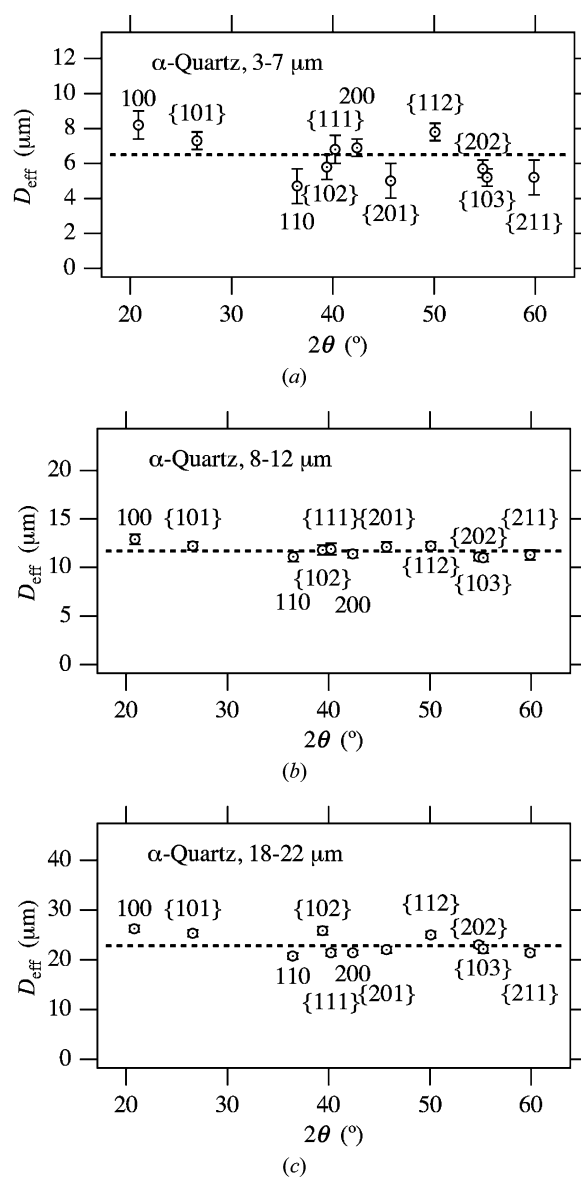


Figure 8 Effective diameters D_{eff} evaluated for (a) 3–7 μm , (b) 8–12 μm and (c) 18–22 μm fractions of quartz powder. The values evaluated for each reflection are plotted as circles, and the weighted average values, 6.5 (2), 11.7 (2) and 22.8 (2) μm , respectively, are shown as broken lines.

Table 4

Results of spinner-scan measurements for the nominally 3–7 μm fraction of quartz powder.

See Table 3 for definitions.

<i>hkl</i>	2θ		$(\Delta I_{\text{obs}})^2$	$(\Delta I_{\text{particle}})^2$	n_{eff}	D'_{eff} (μm)	D_{eff} (μm)
	($^\circ$)	$\langle l \rangle$					
100	20.77	904 (2)	1180 (80)	280 (80)	2960 (870)	5.6 (5)	8.2 (8)
101/011	26.56	2032 (3)	3000 (200)	990 (200)	4170 (870)	5.4 (4)	7.3 (5)
110	36.46	636 (1)	710 (50)	80 (50)	5400 (3600)	3.8 (8)	4.7 (1.0)
102/012	39.38	824 (2)	1020 (70)	190 (70)	3500 (1300)	4.7 (6)	5.8 (7)
111/11 $\bar{1}$	40.23	752 (2)	940 (70)	190 (70)	3000 (1000)	5.6 (7)	6.8 (8)
200	42.37	661 (2)	1000 (70)	340 (70)	1300 (280)	5.8 (4)	6.9 (5)
201/021	45.71	737 (1)	840 (60)	100 (60)	5400 (3100)	4.2 (8)	5.0 (1.0)
112/11 $\bar{2}$	50.06	717 (2)	1090 (70)	370 (70)	1390 (270)	6.8 (4)	7.8 (5)
202/022	54.79	751 (2)	990 (70)	240 (70)	2390 (660)	5.1 (5)	5.7 (5)
103/013	55.24	802 (2)	1120 (90)	320 (90)	2020 (560)	4.6 (4)	5.2 (5)
211/121	59.87	993 (2)	1130 (80)	130 (80)	7300 (4300)	4.6 (9)	5.2 (1.0)

Table 5

Results of spinner-scan measurements for the nominally 8–12 μm fraction of quartz powder.

See Table 3 for definitions.

<i>hkl</i>	2θ		$(\Delta I_{\text{obs}})^2$	$(\Delta I_{\text{particle}})^2$	n_{eff}	D'_{eff} (μm)	D_{eff} (μm)
	($^\circ$)	$\langle l \rangle$					
100	20.79	825 (5)	2200 (150)	1250 (150)	750 (90)	8.8 (3)	12.9 (5)
101/011	26.56	1641 (8)	6840 (490)	4760 (490)	920 (100)	9.0 (3)	12.2 (4)
110	36.46	550 (4)	1730 (150)	1070 (150)	410 (60)	9.0 (4)	11.1 (5)
102/012	39.40	795 (7)	1440 (110)	850 (110)	410 (50)	9.7 (4)	11.8 (5)
111/11 $\bar{1}$	40.21	739 (4)	1380 (110)	740 (110)	560 (80)	9.9 (5)	11.9 (6)
200	42.37	560 (4)	2190 (150)	1520 (150)	290 (30)	9.5 (3)	11.4 (4)
201/021	45.71	673 (4)	2290 (170)	1540 (170)	370 (40)	10.3 (4)	12.1 (5)
112/11 $\bar{2}$	50.06	636 (5)	2180 (150)	1450 (150)	360 (40)	10.6 (4)	12.2 (4)
202/022	54.79	663 (6)	2550 (180)	1780 (180)	330 (30)	9.7 (3)	11.1 (4)
103/013	55.25	629 (6)	2360 (190)	1740 (190)	220 (20)	9.7 (3)	11.0 (4)
211/121	59.88	978 (5)	2390 (190)	1390 (190)	720 (100)	10.0 (5)	11.3 (5)

Table 6

Results of spinner-scan measurements for the nominally 18–22 μm fraction of quartz powder.

See Table 3 for definitions.

<i>hkl</i>	2θ		$(\Delta I_{\text{obs}})^2$	$(\Delta I_{\text{particle}})^2$	n_{eff}	D'_{eff} (μm)	D_{eff} (μm)
	($^\circ$)	$\langle l \rangle$					
100	20.80	968 (2)	8260 (600)	7430 (600)	91 (7)	17.8 (5)	26.2 (7)
101/011	26.57	2086 (4)	27700 (2100)	26000 (2100)	103 (9)	18.6 (5)	25.3 (7)
110	36.47	660 (2)	5330 (440)	4780 (440)	63 (6)	16.7 (6)	20.7 (6)
102/012	39.40	591 (2)	16900 (1500)	16100 (1500)	39 (4)	21.3 (7)	25.8 (8)
111/11 $\bar{1}$	40.22	643 (2)	6340 (570)	5600 (570)	98 (10)	17.7 (6)	21.4 (7)
200	42.38	668 (2)	7570 (530)	7000 (530)	45 (4)	17.9 (4)	21.4 (5)
201/021	45.72	756 (2)	7840 (690)	7170 (690)	63 (6)	18.7 (6)	22.0 (7)
112/11 $\bar{2}$	50.08	727 (2)	10000 (840)	9400 (840)	43 (4)	21.7 (6)	25.0 (7)
202/022	54.80	770 (3)	12400 (890)	11740 (890)	37 (3)	20.2 (5)	23.0 (6)
103/013	55.26	616 (2)	15100 (1500)	14500 (1500)	27 (3)	19.4 (7)	22.1 (8)
211/121	59.88	1001 (2)	9900 (1700)	8920 (700)	107 (8)	19.0 (5)	21.4 (6)

be overestimated, which may be caused by an error in the extrapolation of the calibration curve.

It seems that the errors estimated based on the propagation from the value calculated by equation (21) are slightly underestimated, but acceptable for the results of the 3–7 and 8–12 μm fractions of the quartz samples. The uncertainties in D_{eff} evaluated for the 18–22 μm quartz sample may be partly caused by the small number of diffracting crystallites n_{eff} .

ranging only from 27 to 107 for the applied measurement conditions. It is suggested that accuracy in size estimation for large crystallites will be improved by expanding the irradiated volume V or enhancing the probability p , which may be achieved by changing the measurement conditions.

Even though the calibration formula given by equation (26) does not have a fully concrete theoretical basis, it can be concluded that the dependence on the diffraction angle has been successfully removed.

The weighted average values of \bar{D}_{eff} are estimated at 6.5 (2), 11.7 (2) and 22.8 (2) μm for the 3–7, 8–12 and 18–22 μm fractions of quartz powder, while the values estimated by the SEM image analysis were 7.1, 11.8 and 25.3 μm . Any discrepancy might be caused by the assumptions of the SEM image analysis rather than the analysis of the spinner-scan data. NIST SRM640c Si powder might not be an ideal material as the standard for evaluation of particle statistics, because of the irregular shape and broad size distribution, as can be seen in the SEM image (Fig. 1). It is expected that a more reliable analysis could be achieved if a standard crystalline powder with a more regular shape and narrower size distribution were available.

The method will also be applicable to a parallel-beam geometry using synchrotron or multilayer mirror optics, if the effective focal size is evaluated using a standard powder. Use of synchrotron X-rays may expand the sensitivity of the method to smaller crystallite sizes, because a smaller focal size is expected for a synchrotron X-ray source.

3.4. Possible applications of the spinner-scan method

The results of the current study show that the effective number of crystallites n_{eff} that satisfy the diffraction condition can certainly be measured, simply by rotating the specimen stepwise and recording the diffraction peak intensities.

As has been suggested in §3.2, information on the multiplicity of the measured reflection can be obtained experimentally by this method without any preliminary knowledge of crystal symmetry or atomic arrangements.

The effective multiplicity of reflection is formally calculated by

$$m_{\text{eff}} = n_{\text{eff}} \mu_0 D_{\text{eff}}^3 f(\theta), \quad (28)$$

$$f(\theta) = \frac{4\pi^2 R \sin \theta}{3A_w \Phi_A} \left[\frac{(D'_{\text{eff}})_{\text{fit}}}{(D_{\text{eff}})_{\text{Si}}} \right]^3, \quad (29)$$

where the calibration curve $f(\theta)$ is determined by the measurement of the standard sample. The formula for $f(\theta)$ applied in this study is simplified as

$$f(\theta) = \sin \theta / [(138 \mu\text{m}^2)(0.62 / \tan \theta - 0.41 + 1.33 \tan \theta)]. \quad (30)$$

Note that the effective number of diffracting crystallites is straightforwardly evaluated by the spinner-scan measurement as $n_{\text{eff}} = \langle l \rangle^2 / (\Delta I_{\text{particle}})^2$. The absorption coefficient μ_0 is obtained from the chemical composition and the density. Then, the value of the multiplicity of reflection m_{eff} can be

calculated using equation (28) if only the crystallite size D_{eff} is determined.

The experimental values of m_{eff} , calculated for Si and the 8–12 μm fraction of the quartz powder sample using equations (28) and (30), and the values predicted by the known crystal structures, are plotted in Fig. 9. The values of the effective diameter $D_{\text{eff}} = 5.6$ and 12 μm , determined by SEM image analysis for the Si and quartz samples, respectively, are used for the calculation.

Even though the calibration curve has been adjusted for the Si data, the good coincidence between the predicted and observed values of m_{eff} shown in Fig. 9(a) indicates that the relative values of the effective multiplicity m_{eff} can be experimentally evaluated by this method without any standard samples or knowledge of particle size.

The values of m_{eff} for the 8–12 μm quartz powder evaluated by the spinner-scan measurement coincide absolutely with the values predicted by the crystal structure, almost within the experimental errors, as can be seen in Fig. 9(b). This means that the absolute value of the multiplicity of reflection can be evaluated by this method without any knowledge of the crystal structure, when the effective crystallite diameter is known. Evaluation of the relative values of m_{eff} will be much easier, because the values of μ_0 and D_{eff} are not needed. It is thus expected that the method will provide valuable information on the determination of an unknown structure.

The results presented in §3.3 show that crystallite sizes over a range of several micrometres, which cannot be evaluated by

line-broadening analysis, can certainly be evaluated by the spinner-scan method. The values for different diffraction peaks coincide well for all the samples examined in this study. This means that the evaluation can be completed by measurement of the strongest diffraction peak, which will only take a few minutes, when a random orientation of the crystallites can be assumed.

It is further suggested that the preferred orientation of crystallites may also be evaluated by this method, simply by measuring different diffraction peaks, because the number of diffracting crystallites n_{eff} for each reflection should in principle be exactly proportional to the probability that the normal direction of the diffraction plane coincides with the direction normal to the face of the specimen.

Since the analysis of spinner-scan data provides additional information almost independent of that included in one-dimensional powder diffraction data, application of the method can refine any results of an analysis based on powder diffraction data. For example, the method can be used to test the validity of structure models from indexing and structure analysis, and to distinguish a strong impurity diffraction peak from weak main-phase diffraction peaks in multiphase mixtures by the different numbers of diffracting crystallites n_{eff} .

Finally, the authors would like to note that the spinner-scan method is applicable not only to powder samples but also to polycrystalline materials for practical use, such as sintered ceramics or alloys.

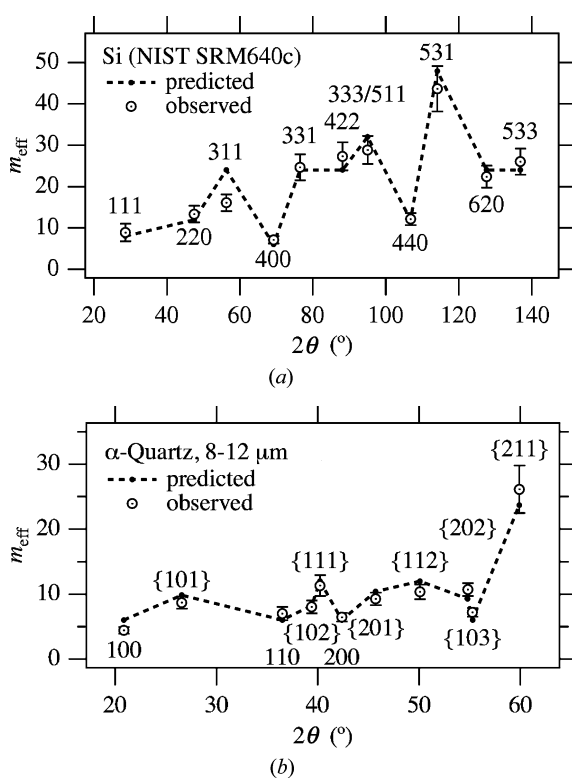


Figure 9 Effective multiplicity of reflection m_{eff} for (a) Si and (b) 8–12 μm quartz samples, as predicted by the known crystal structure (dots connected with broken lines) and as evaluated by the spinner-scan measurement (open circles).

4. Conclusions

The statistical properties of powder X-ray diffraction intensities measured by a step scan about the rotation angle of a specimen-spinning attachment have been investigated.

The results show that the statistical variance assigned to particle statistics can be quantitatively evaluated by this method, and estimation of crystallite size over a range of several micrometres, which is practically impossible by conventional methods based on line-broadening analysis, has been achieved at considerable accuracy.

It is also suggested that the method is useful for various applications based on powder diffractometry, including determination of unknown structures, structure refinement, evaluation of preferred orientation, and qualitative and quantitative analysis of multiphase mixtures.

APPENDIX A Modified Γ distribution

The probability density function of the modified Γ distribution for diameter D used in this study is given by

$$f_{\Gamma W}(D) = \frac{\beta}{\Gamma(\alpha)D_0} \left(\frac{D}{D_0}\right)^{\alpha\beta-1} \exp\left[-\left(\frac{D}{D_0}\right)^\beta\right]. \quad (31)$$

The average value of D^j for the distribution is obtained by solving the equation

$$\langle D^j \rangle_{\Gamma W} = \int_0^{\infty} D^j f_{\Gamma W}(D) dD, \quad (32)$$

which gives

$$\langle D^j \rangle_{\Gamma W} = \Gamma(\alpha + j/\beta) D_0^j / \Gamma(\alpha). \quad (33)$$

The effective diameter for particle statistics in the modified Γ -distribution model is given by

$$D_{\text{eff}} = \left(\frac{\langle D^6 \rangle}{\langle D^3 \rangle} \right)^{1/3} = D_0 \left[\frac{\Gamma(\alpha + 6/\beta)}{\Gamma(\alpha + 3/\beta)} \right]^{1/3}. \quad (34)$$

The formula for $f_{\Gamma W}(D)$ is reduced to the usual Γ distribution

$$f_{\Gamma}(D) = \frac{1}{\Gamma(\alpha) D_0} \left(\frac{D}{D_0} \right)^{\alpha-1} \exp\left(-\frac{D}{D_0}\right) \quad (35)$$

for $\beta = 1$, and to the Weibull distribution

$$f_W(D) = \frac{\beta}{D_0} \left(\frac{D}{D_0} \right)^{\beta-1} \exp\left[-\left(\frac{D}{D_0}\right)^{\beta}\right] \quad (36)$$

for $\alpha = 1$.

The relative volume fraction based on the distribution is derived by solving

$$F(D) = \langle D^3 \rangle_{\Gamma W}^{-1} \int_0^D t^3 f_{\Gamma W}(t) dt, \quad (37)$$

which gives

$$F(D) = P[\alpha + 3/\beta; (D/D_0)^{\beta}]. \quad (38)$$

APPENDIX B

Properties of log-normal distribution

The probability density function of the log-normal distribution for diameter D is given by

$$f_{\text{LN}}(D; D_m, \omega) = \frac{1}{(2\pi)^{1/2} \omega} \exp\left[-\frac{(\ln D - \ln D_m)^2}{2\omega^2}\right]. \quad (39)$$

The average of D^j is given by solving the equation

$$\langle D^j \rangle = \int_0^{\infty} D^j f_{\text{LN}}(D; D_m, \omega) dD, \quad (40)$$

which gives

$$\langle D^j \rangle = D_m^j \exp(j^2 \omega^2 / 2). \quad (41)$$

The effective diameter for particle statistics in the log-normal distribution model is then given by

$$D_{\text{eff}} = (\langle D^6 \rangle / \langle D^3 \rangle)^{1/3} = D_m \exp(9\omega^2 / 2). \quad (42)$$

The relative volume fraction for the log-normal distribution is derived by solving

$$F(D) = \langle D^3 \rangle_{\text{LN}}^{-1} \int_0^D t^3 f_{\text{LN}}(t) dt, \quad (43)$$

which gives

$$F(D) = \frac{1}{2} \left[1 + \operatorname{erf}\left(\frac{\ln D - \ln D_m - 3\omega^3}{2^{1/2}\omega}\right) \right]. \quad (44)$$

References

- Alexander, L., Klug, H. P. & Kummer, E. (1948). *J. Appl. Phys.* **19**, 742–753.
- De Wolff, P. M. (1958). *Appl. Sci. Res.* **7**, 102–112.
- Freiman, S. W. & Trahey, N. M. (2000). Certificate Standard Reference Material 640c. National Institute of Standards and Technology, Gaithersburg, USA.
- Ida, T. (2008). *J. Appl. Cryst.* **41**, 1019–1023.
- Ida, T. & Toraya, H. (2002). *J. Appl. Cryst.* **35**, 58–68.
- Izumi, F. & Ikeda, T. (2000). *Mater. Sci. Forum.* **321–324**, 198–203.
- Smith, D. K. (2001). *Powder Diffract.* **16**, 186–191.
- Teich, M. C. (1985). *Biol. Cybern.* **53**, 121–124.